Fundamental Three Dimensional Modeling and Parameter Estimation of a Diesel Oxidation Catalyst for Heavy Duty Trucks

A. Holmqvist[1] and I. Odenbrand[1*]
[1]Department of Chemical Engineering, Faculty of Engineering LTH, Lund University
*Corresponding author: P.O. Box 124, SE-221 00 Lund, Sweden, Ingemar.Odenbrand@chemeng.lth.se

Abstract: Numerical investigation of the catalytic monolithic converter (Pt/Al_2O_3 in oxygen rich exhaust) during highly dynamic conditions is addressed. A fundamental model was developed to incorporate a qualitative description of this process. To quantitatively gain an accurate prediction of the exhaust gas composition kinetics steps of heterogeneous reactions over platinum were set up. A method to estimate and analyze the kinetic parameters of the mean field model from transient flow experiments by inverse modeling is proposed. These problems are known to be ill-conditioned and multimodal. Thus, indirect local optimization methods fail to give satisfactory solutions. To surmount this limitation, the use of a stochastic global optimization method, evolution strategy (ES), is presented. Sensitivity analysis was also performed to assess the relative importance of each reaction in determining the conversion.

Keywords: Diesel oxidation catalyst; Inverse modeling; Parameter estimation ; Evolution strategy; Sensitivity analysis

1. Introduction

Mathematical optimization can be used as a computational engine to generate the best solution for a given problem in a systematic and efficient way. In the context of monolithic converter systems, the parameter estimation problem (or inverse problem) is solved using partial differential equations (PDE)-based models of the physical system coupled with an optimization algorithm. These problems are usually underdetermined due to the lack of enough data to constrain a unique solution. Inverse modeling refers to the practice of using given experimental data to calibrate the model so as to reproduce the experimental results in the best way possible. The exact solution of inverse problems plays a key role in the development of dynamic models, which in turn can promote functional understanding at the system level.

If, reliable models were available to the industry, new exhaust line configurations could be tested rapidly and inexpensively [1]. In the last years, several models were proposed for the numerical simulation of catalytic converters reaching from a one-dimensional up to a three-dimensional description [2, 3].

2. Theory

Common washcoat application methods leave most of the material in the corners, thus the assumption of an evenly distributed washcoat will be inaccurate. R.E. Hayes et al. [4] have proven that it is crucial to implement a geometric monolith structure which represents the real appearance of the Diesel Oxidation Catalyst, DOC. Due to symmetry; the model domain Ω was reduced to a long prism cutting through one unit cell, cf. Figure 1. The structure of the catalytic converter dictates splitting the model problem into two distinct and connected sub domains, one for the channel and one for the porous catalytic washcoat. The transformation from reactants to products involves transport of reactants by convective flow in the free channel and molecular diffusion towards the walls and into the porous washcoat, within which diffusion and surface reactions occur. Formed products subsequently diffuse out of the porous structure and are transported out of the reactor through the free channel. The mathematical theory and the scope of simulation given in C. Brinkmeier [5] and T.G. Chuah et al. [2], laid the foundation of the implemented model.

2.1 Monolithic converter model

The monolithic converter model was based on conservation equations for mass, momentum, energy, and individual gas-phase species along with constitutive relations for momentum, heat, and species fluxes.

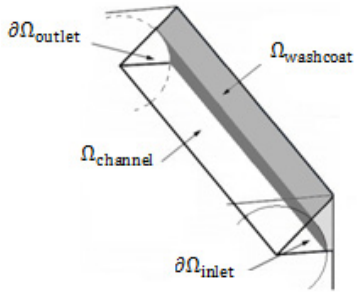

Figure 1. Principle sketch of the domain Ω with the portioned boundary $\partial\Omega = \partial\Omega_{inlet} \cup \partial\Omega_{outlet} \cup \partial\Omega_{wall}$.

These transport equations can be readily found in the fluid dynamics textbook of Bird et al. [6].

The flow in the free channel of the monolith is laminar for the whole range of exhaust gas velocities that are induced by the engine, which motivates a negligible compressibility; therefore the flow in the free channel sub domain was modeled by the incompressible Navier-Stokes equations:

$$\rho\frac{\partial \mathbf{V}}{\partial t} = \nabla\cdot[-p\mathbf{I} + \mu(\nabla\mathbf{V} + (\nabla\mathbf{V})^T)] - \rho(\mathbf{V}\cdot\nabla)\mathbf{V}$$
$$\mathbf{V}\cdot\nabla = 0 \quad (1)$$

where p is the gas pressure, $\mathbf{V}$ the gas velocity vector, μ denotes the dynamic viscosity, the gas density ρ is treated by the ideal gas law, and the incompressibility imposed on the conservation of mass yielded the continuity equation.

In the porous sub domain, the flow variables and fluid properties are averaged over a control volume surrounding a point. This control volume is small compared to the typical macroscopic dimensions of the problem, but large enough to be representative of the averaged porous structure. The Brinkman equations govern the flow in the porous sub domain, for which the momentum transport within the fluid due to shear stresses is of importance:

$$\frac{\rho}{\varepsilon}\frac{\partial \mathbf{v}}{\partial t} = \nabla\cdot\left[-p\mathbf{I} + \frac{\mu}{\varepsilon}(\nabla\mathbf{v} + (\nabla\mathbf{v})^T)\right] - \frac{\mu}{\kappa}\mathbf{v}$$
$$\mathbf{v}\cdot\nabla = 0 \quad (2)$$

where κ denotes the permeability and the porosity ε is assumed to be constant and uniform over the entire washcoat. The flow velocities are defined as superficial volume averages, which are averaged unit volumes of the medium including both pores and matrix. Such a definition makes the velocity field continuous across the boundary between the porous and the free channel sub domain.

As for the temperature field, the energy balance in the free channel sub domain was implemented accordingly:

$$\rho\, C_p\frac{\partial T}{\partial t} = +\nabla\cdot(k\nabla T) - \rho\, C_p\mathbf{V}\cdot\nabla T \quad (3)$$

where T is the temperature, C_p and k denotes the specific heat and thermal conductivity respectively. In the porous sub domain, the energy equation can be expressed with a single temperature variable, defined per unit volume of the medium, following the assumption that the pore fluid and solid matrix quickly reaches thermal equilibrium:

$$(\rho C_p)^s\frac{\partial T^s}{\partial t} = \nabla\cdot(k^s\nabla T^s) - \rho C_p\mathbf{v}\cdot\nabla T^s + (1-\varepsilon)A_s\sum_j^{N_j} r_j\left(-\Delta H_j\right) \quad (4)$$

where the effective heat capacity $(\rho C_p)^s$ and the thermal conductivity k^s are porosity, weighted functions of the gas and the solid phase properties. The Arrhenius type reaction rate expressions r_j of the micro kinetic model are presented in Table 2.

For the free-flow sub domain, the mass balance gives the following convection and diffusion transport equations for the molar concentrations c_i:

$$\frac{\partial c_i}{\partial t} = \nabla\cdot(D_i\nabla c_i - c_i\mathbf{V}) \quad (5)$$

In the porous sub domain, the molar concentration c_i^s represents the intrinsic volume-averaged molar concentration of the species. The resulting mass balance for the porous sub domain is:

$$\varepsilon\frac{\partial c_i^s}{\partial t} = \nabla\cdot(\varepsilon D_i^s\nabla c_i^s) - \nabla\cdot(c_i^s\mathbf{v}) + (1-\varepsilon)A_s\sum_j^{N_j} v_{ij}r_j \quad (6)$$

where $\mathbf{v}$ is the superficial volume-average velocity vector of the mixture and D_i^s the effective diffusion coefficient in the complex pore system, which depends on the bulk diffusion coefficient and the porosity of the washcoat [7]. Using the values of the transport properties of the constituent species, the transport properties of the gas mixture were estimated from empirical mixture rules [8] and thermodynamic data [9].

The DOC model is subject to the following boundary conditions: At $\partial\Omega_{\text{inlet}}$ the normal inflow velocity, the concentrations and temperature are prescribed (Dirichlet boundary conditions), and at $\partial\Omega_{\text{insulating}}$ the velocity is zero and the concentrations and temperature fluxes are zero (Dirichlet and Neumann boundary conditions, respectively), and at $\partial\Omega_{\text{symmetry}}$ the no penetration and vanishing shear stress as well as the concentrations and temperature fluxes are prescribed to zero (Neumann boundary conditions), and at $\partial\Omega_{\text{interior}}$ continuity conditions are imposed, which assures that the fluxes in the normal direction are continuous across the boundary, and at $\partial\Omega_{\text{outlet}}$ is a free boundary the pressure and normal stress as well as the diffusive concentration and conductive temperature fluxes are prescribed to zero (Dirichlet and Neumann boundary conditions, respectively). The mathematical descriptions of the boundary conditions are presented in Table 1.

2.1 Micro kinetic model

One of the most common ways to describe the surface reactions and the adsorption/desorption is the mean-field approach, where the reactions are average over the whole catalyst surface. The mean-field kinetic model, with 7 reacting species and 17 heterogeneous reactions, was described by Crocoll et al. [10] and Olsson et al. [11]. The reactions rate equations, presented in Table 2, are dependent on non-mobile surface fractional coverage θ_i for species i defined accordingly:

$$\Gamma_{cat}\frac{\partial\theta_i}{\partial t} = A_s\sum_j^{N_j} v_{ij}r_j \tag{7}$$

The initial surface coverage's were calculated from the Langmuir equilibrium isotherm equation stated as:

$$\theta_i = \frac{(K_i c_i)^{\frac{1}{n}}}{1+\sum_i^{N_i}(K_i c_i)^{\frac{1}{n}}} \tag{8}$$

where K_i is the quotient of the adsorption and desorption rate constants and n denotes the number of surface Pt-sites that the species chemisorbs to.

2.2.1 Formulation of the inverse optimization problem

The correct solution of inverse problems plays a key role in the development of dynamic models, which, in turn, can promote functional understanding at the systems level. Parameter estimation problems of nonlinear dynamic systems are stated as minimizing a cost function that measures the goodness of the fit of the model with respect to a given experimental data set.

The inverse parameter estimation is formulated here as a nonlinear optimization problem, where the mean field model´s kinetic parameters are calibrated by minimizing a suitable objective function based on the deviations between observed and predicted system response. The optimization process used includes three basic steps repeated until some predefined convergence criteria are satisfied. These steps are: (i) parameter perturbation, (ii) forward modeling; (iii) objective function evaluation.

The formulation of the objective function (or misfit function) from the maximum likelihood theory leads to a weighted least squares problem, taking the form:

$$Q(\boldsymbol{x}) = \sum_{j=1}^{n}\sum_{i=1}^{m} W_{i,j}\left\{\left[y_{pred}(\boldsymbol{x},i) - y_{obs}(i)\right]_j\right\}^2 \tag{9}$$

where the right-hand-side represents the deviation between the model-predicted y_{pred} and the corresponding observed y_{obs} mean gas channel composition at the outlet ($\partial\Omega_{\text{outlet}}$), using the calibration parameters $\boldsymbol{x}$. n is the number of measurements over time within a particular set corresponding to the concentration of species j, while m denotes the number of different species. $W_{i,j}$ corresponds to the different weights taken to normalize the contributions of each particular measurement.

2.2.2 Global optimization

The optimization algorithm finds the optimum of the objective function $Q(\boldsymbol{x})$ with upper and lower boundaries (UB and LB) on the calibration parameters $\boldsymbol{x}$. With the above calibration parameters and constraints, the optimization problem is stated as the minimization of a weighted distance measure:

$$Q_{\min} = \min_{LB\leq xUB}\left(Q(\boldsymbol{x})\right) \tag{10}$$

Because of the nonlinear, non-differentiable and constrained nature of the system dynamics, the problem is multimodal (non convex). Therefore, if the optimization problem is solved via local direct search methods, it is very likely that the solution found will be of local nature. One approach to surmount the non convexity of the optimization problems is the so-called multistart strategy, which uses a local method repeatedly, starting from a number of different initial decision vectors. However, this method becomes very inefficient, since the same minimum will eventually be determined several times, and global optimization methods which ensure better efficiency and robustness are preferably used instead [12].

Global optimization methods can be roughly classified as deterministic and stochastic strategies. Stochastic methods for global optimization ultimately rely on probabilistic approaches. Given that random elements are involved, these methods only have weak theoretical guarantees of convergence to the global solution. However, in practice, one can be satisfied if these methods provide a very good solution in modest computation times. Furthermore, stochastic methods are usually quite simple to implement and use, and they do not require transformation of the original problem, which can be treated as a black box. This characteristic is especially interesting because very often the optimizer must be linked with a separate software package in which the process dynamic model has been implemented.

Table 1. Boundary conditions for the monolithic converter model governing equations.

	Mass	Momentum	Heat
Inlet	$c_i = c_{i,0}$	$\mathbf{V}\cdot\mathbf{n} = V_0$	$T = T_0$
Outlet	$\mathbf{n}\cdot(-D_i\nabla c_i) = 0$	$\mathbf{n}\cdot[-p\mathbf{I}+\mu(\nabla\mathbf{V}+(\nabla\mathbf{V})^T)] = 0, p = p_0$	$\mathbf{n}\cdot(-k\nabla T) = 0$
Interior[1]	$\mathbf{n}\cdot(-D_i\nabla c_i + c_i\mathbf{V}) = \mathbf{n}\cdot(-\varepsilon D_i^s\nabla c_i^s + c_i^s\mathbf{v})$	$\mathbf{n}\cdot[\mu(\nabla\mathbf{V}+(\nabla\mathbf{V})^T)] = \mathbf{n}\cdot\left[\frac{\mu}{\varepsilon}(\nabla\mathbf{v}+(\nabla\mathbf{v})^T)\right]$	$\mathbf{n}\cdot(-k\nabla T+\rho C_p T\mathbf{V}) = \mathbf{n}\cdot(-k^s\nabla T^s+\rho C_p T^s\mathbf{v})$
Symmetry	$\mathbf{n}\cdot(-D_i\nabla c_i + c_i\mathbf{V}) = 0$	$\mathbf{V}\cdot\mathbf{n} = 0, \mathbf{t}\cdot[-p\mathbf{I}+\mu(\nabla\mathbf{V}+(\nabla\mathbf{V})^T)]\mathbf{n} = 0$	$\mathbf{n}\cdot(-k\nabla T+\rho C_p T\mathbf{V}) = 0$
Insulating	$\mathbf{n}\cdot(-D_i\nabla c_i + c_i\mathbf{V}) = 0$	$\mathbf{V} = 0$	$\mathbf{n}\cdot(-k\nabla T+\rho C_p T\mathbf{V}) = 0$

[1]Washcoat/Channel boundary

Table 2. Kinetic parameters of the NO, CO and C_3H_6 oxidation over the Pt/Al_2O_3 catalyst [10,11] and the determined calibration parameters.

Reaction	Reaction rate	Parameter		Value	Parameter estimation
Adsorption					
$O_{2(g)} + 2* \overset{r_1}{\rightarrow} 2O*$	$r_1 = A_1 \exp\left(-\frac{E_1}{RT}\right) c_{O_2(g)} \theta_*^2$	A_1	$(m^3 s^{-1} m^{-2})$	11	$4.2 \cdot 10^1$
		E_1	$(kJmol^{-1})$	0	
$NO_{(g)} + * \overset{r_3}{\rightarrow} NO*$	$r_3 = A_3 \exp\left(-\frac{E_3}{RT}\right) c_{NO(g)} \theta_*$	A_3	$(m^3 s^{-1} m^{-2})$	138	$1.69 \cdot 10^1$
		E_3	$(kJmol^{-1})$	0	
$NO_{2(g)} + * \overset{r_5}{\rightarrow} NO_2*$	$r_5 = A_5 \exp\left(-\frac{E_5}{RT}\right) c_{NO_2(g)} \theta_*$	A_5	$(m^3 s^{-1} m^{-2})$	68	$1.71 \cdot 10^1$
		E_5	$(kJmol^{-1})$	0	
$CO_{(g)} + * \overset{r_7}{\rightarrow} CO*$	$r_7 = A_7 \exp\left(-\frac{E_7}{RT}\right) c_{CO(g)} \theta_*$	A_7	$(m^3 s^{-1} m^{-2})$	141	
		E_7	$(kJmol^{-1})$	0	
$CO_{2(g)} + * \overset{r_9}{\rightarrow} CO_2*$	$r_9 = A_9 \exp\left(-\frac{E_9}{RT}\right) c_{CO_2(g)} \theta_*$	A_9	$(m^3 s^{-1} m^{-2})$	0.67	
		E_9	$(kJmol^{-1})$	0	
$H_2O_{(g)} + * \overset{r_{11}}{\rightarrow} H_2O*$	$r_{11} = A_{11} \exp\left(-\frac{E_{11}}{RT}\right) c_{H_2O(g)} \theta_*$	A_{11}	$(m^3 s^{-1} m^{-2})$	157	
		E_{11}	$(kJmol^{-1})$	0	
Desorption					
$2O* \overset{r_2}{\rightarrow} O_{2(g)} + 2*$	$r_2 = A_2 \exp\left(-\frac{E_2(1-\alpha_2\theta_O)}{RT}\right) \theta_O^2$	A_2	$(mols^{-1} m^{-2})$	$2 \cdot 10^{10}$	$1.31 \cdot 10^{10}$
		$E_2(0)$	$(kJmol^{-1})$	200	
		α_2	$(-)$	0.10	$2.51 \cdot 10^{-1}$
$NO* \overset{r_4}{\rightarrow} NO_{(g)} + *$	$r_4 = A_4 \exp\left(-\frac{E_4 - \alpha_4\theta_O}{RT}\right) \theta_{NO}$	A_4	$(mols^{-1} m^{-2})$	$2 \cdot 10^{11}$	$7.57 \cdot 10^{11}$
		$E_4(0)$	$(kJmol^{-1})$	114	
		α_4	$(kJmol^{-1})$	10	$3.47 \cdot 10^2$
$NO_2* \overset{r_6}{\rightarrow} NO_{2(g)} + *$	$r_6 = A_6 \exp\left(-\frac{E_6(1-\alpha_6\theta_O)}{RT}\right) \theta_{NO_2}$	A_6	$(mols^{-1} m^{-2})$	$2 \cdot 10^8$	$9.28 \cdot 10^7$
		$E_6(0)$	$(kJmol^{-1})$	72	
		α_6	$(-)$	0.075	$4.37 \cdot 10^{-2}$
$CO* \overset{r_8}{\rightarrow} CO_{(g)} + *$	$r_8 = A_8 \exp\left(-\frac{E_8 - \alpha_8\theta_{CO}}{RT}\right) \theta_{CO}$	A_8	$(mols^{-1} m^{-2})$	$2 \cdot 10^{11}$	
		$E_8(0)$	$(kJmol^{-1})$	146	
		α_8	$(kJmol^{-1})$	33	
$CO_2* \overset{r_{10}}{\rightarrow} CO_{2(g)} + *$	$r_{10} = A_{10} \exp\left(-\frac{E_{10}}{RT}\right) \theta_{CO_2}$	A_{10}	$(mols^{-1} m^{-2})$	$2 \cdot 10^8$	
		E_{10}	$(kJmol^{-1})$	27	
$H_2O* \overset{r_{12}}{\rightarrow} H_2O_{(g)} + *$	$r_{12} = A_{12} \exp\left(-\frac{E_{12}}{RT}\right) \theta_{H_2O}$	A_{12}	$(mols^{-1} m^{-2})$	$2 \cdot 10^8$	
		E_{12}	$(kJmol^{-1})$	40	
Surface reactions					
$NO_{(g)} + O* \overset{r_{13}}{\rightarrow} NO_2*$	$r_{13} = A_{13} \exp\left(-\frac{E_{13} - \alpha_{13}\theta_O}{RT}\right) c_{NO(g)} \theta_O$	A_{13}	$(m^3 s^{-1} m^{-2})$	104	$7.25 \cdot 10^1$
		$E_{13}(0)$	$(kJmol^{-1})$	35	
		α_{13}	$(kJmol^{-1})$	14	25.03
$NO_2* \overset{r_{14}}{\rightarrow} NO_{(g)} + O*$	$r_{14} = A_{14} \exp\left(-\frac{E_{14}}{RT}\right) \theta_{NO_2}$	A_{14}	$(mols^{-1} m^{-2})$	$2 \cdot 10^8$	
		E_{14}	$(kJmol^{-1})$	51	
$CO* + O* \overset{r_{15}}{\rightarrow} CO_2* + *$	$r_{15} = A_{15} \exp\left(-\frac{E_{15} - \alpha_{15}\theta_{CO}}{RT}\right) \theta_{CO} \theta_O$	A_{15}	$(mols^{-1} m^{-2})$	$4 \cdot 10^4$	
		$E_{15}(0)$	$(kJmol^{-1})$	108	
		α_{15}	$(mols^{-1} m^{-2})$	33	
$CO_2* + * \overset{r_{16}}{\rightarrow} CO* + O*$	$r_{16} = A_{16} \exp\left(-\frac{E_{16} + \alpha_{16}\theta_O}{RT}\right) \theta_{CO_2} \theta_*$	A_{16}	$(mols^{-1} m^{-2})$	$2 \cdot 10^8$	
		$E_{16}(0)$	$(kJmol^{-1})$	155	
		α_{16}	(kJ/mol)	45	
$\frac{1}{3} C_3H_{6(g)} + 3O* \overset{r_{17}}{\rightarrow} CO_{2(g)} + H_2O_{(g)}$	$r_{17} = A_{17} \exp\left(-\frac{E_{17} - \alpha_{17}\theta_O}{RT}\right) c_{CH_2} \theta_O$	A_{17}	$(m^3 s^{-1} m^{-2})$	104	$1.75 \cdot 10^{10}$
		$E_{17}(0)$	(kJ/mol)	95	
		α_{17}	(kJ/mol)	45	$7.10 \cdot 10^3$

There exists several stochastic methods for global optimization, and the one used in this paper is the Differential Evolution (DE) method as presented by Storn and Price [13, 14]. The DE algorithm is a population based algorithm like genetic algorithms using the similar operators; crossover, mutation and selection. The main difference in constructing better solutions is that genetic algorithms rely on crossover while DE relies on mutation operation. This main operation is based on the differences of randomly sampled pairs of solutions in the population. The algorithm uses mutation operation as a search mechanism and selection operation to direct the search toward the prospective regions in the search space. The DE algorithm also uses a non-uniform crossover that can take child vector parameters from one parent more often than it does from others. By using the components of the existing population members to construct trial vectors, the recombination (crossover) operator efficiently shuffles information about successful combinations, enabling the search for a better solution space [15, 16].

2.2.3 Calibration parameters

The main calibration parameters studied were the kinetic parameters of the mean field model, i.e. the pre-exponential factors A_i and the linear activation energy correction factors α_i, presented in Table 2.

Only the kinetic parameters of the individual overall heterogeneous reactions which concern the NO and C_3H_6 oxidation were considered, since no reliable experimental observations were available regarding the CO oxidation. Further, to ensure that the global gas phase equilibrium of the NO oxidation holds in any case, the reaction rate constant k_{14} was calculated from a thermodynamic relationship [17]. Thus, the inverse optimization problem consists of total number of 13 calibration parameters to be determined. The orders of magnitude of the calibration parameters were approximately estimated with micro kinetic analysis [18] and used as initial point.

3. Solution methodology

The commercial finite element software, COMSOL Multiphysics version 3.5a, was used in this study for solving the system of partial differential equations. The ability to interface with programming languages like MATLAB, enables a COMSOL-generating M-file (readable in either MATLAB or COMSOL script) to be converted into a function that may be called as a "black box" by an optimization routine [19]. Running this M-file in MATLAB, the FEM structure is created in MATLAB's workspace, and includes all information about the model's geometry, governing equations, boundary conditions, and solution parameters. This functionality forms the basis of the COMSOL-MATLAB linkage and enables to write MATLAB routines that can extract relevant information from the FEM structure automatically.

In order to solve the inverse problem, MATLAB must be able to recognize which parameters of the COMSOL file it should alter. This was realized through overwriting the constants in the FEM structure [20]. For every calibration variable set (corresponding to one individual in the population) one function evaluation was performed. The outcome of DE is much dependent on the size of the population, due to the weak theoretical guarantees of convergence to the global solution, the bigger the more reliable result. But with large populations the forward model evaluations grows rapidly, and thus the computational time.

The objective function requires the forward model-predicted average gas channel composition at the outlet:

$$\langle c_i \rangle|_{\partial\Omega_{\text{outlet}}} = \frac{1}{A}\int_{\Omega} c_i(t, \boldsymbol{X}) dA \qquad (11)$$

and was evaluated with the post processing function *postint*.

3.1 Implementation

A one-way coupling was assumed such that the momentum Equations (1)-(2) are independent of the concentrations and the temperature governed by Equations (3)-(6). Consequently, a segregated solution method was employed. The resulting system of PDEs was solved using the direct UMFPAK routine on an ordinary PC with a triangular mesh composed of approximately 5500 nodes. The majority of the simulations were completed under 100 s.

4. Results and discussion

The model predicted temporal conversion of the species NO, NO_2 and C_3H_6 were calibrated with transient experimental data set performed at the Department of Chemical Engineering, Faculty of Engineering LTH, Lund University, with a heavy-duty truck engine rig [21]. The initial conditions corresponding to these experimental case studies are presented in Table 2. When using one or two calibration parameters the objective function surface is easy to plot and the optimum can easily be verified. When using multiple calibration parameters, the objective function surface is difficult to visualize and another method has to be used. The optima were verified by plotting the variation in the objective function as a function of each calibration parameters. Figure 2 (diagonal) shows the convergence process for the kinetic parameters regarding the NO oxidation when calibrated with the (750/250) experimental data set using 500 individuals and 30 iterations. The convergence process pattern gives perspective of the calibration parameters sensitivity. An insensitive calibration variable provides the same contribution to the stated objective function for different values. According to the Figure 2, parameters A_4 and α_4 demonstrated no systematical convergence pattern in contrast to parameters A_{13} and α_{13}. One main advantage of the DE algorithm, is that objective function insensitive calibration parameters don't affect the convergence in a negative manner as they would with an indirect optimization method.

The plots below the diagonal in Figure 2 show the kinetic parameters intercorrelation.

Table 3. Initial values of the experimental data sets, corresponds to different speed/torque combinations (load points), used to determine the reaction kinetics [21].

Experiment (rpm/Nm)	Flow (kg/h)	Temp (°C)	$[O_2]$ (%)	$[CO_2]$ (%)	$[H_2O]$ (%)	[Ar] (%)	[NO] (ppm)	$[NO_2]$ (ppm)	[CO] (ppm)	$[C_3H_6]$ (ppm)
(750/250)	310	203	14.5	4.2	7.6	0.9	910	55	97	153
(1000/250)	414	221	14.6	4.2	7.6	0.9	671	52	97	148
(1500/250)	673	237	14.7	4	7.3	0.9	572	52	97	156
(2000/250)	986	262	14.5	4.1	7.4	0.9	575	44	92	176

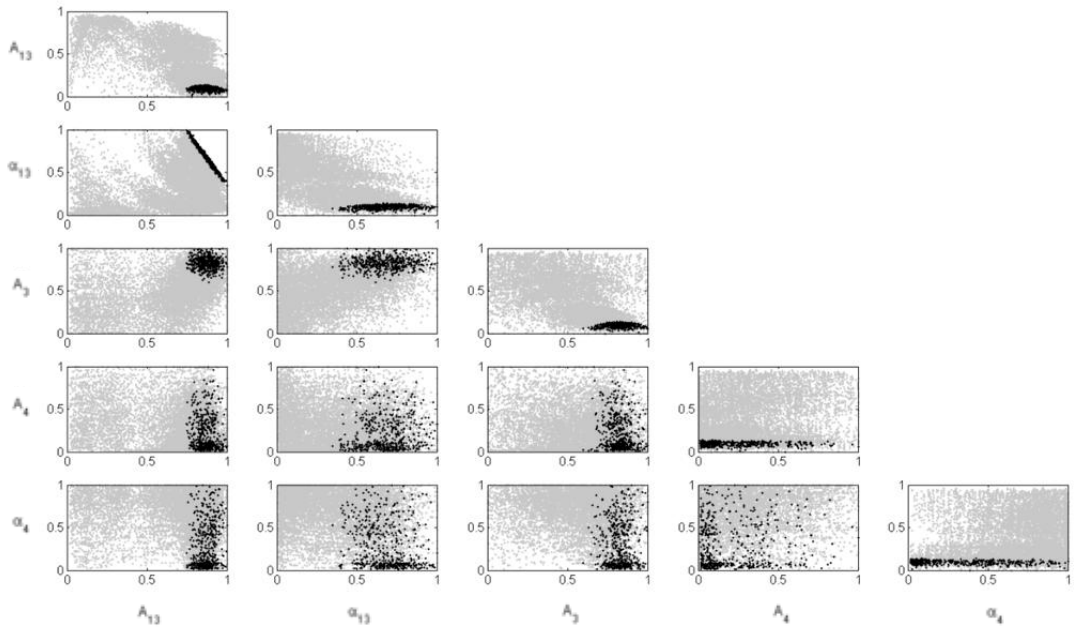

Figure 2. Scatter plots from the case studies used for parameter ranking. Diagonal: Normalized objective function on the y-axis and the normalized parameter variation on the x-axis. The final generation is colored black.

A clear intercorrelation between A_{13} and α_{13} is presented, which is to be expected since they appear in the same Arrhenius-type reaction rate expression. On the contrary, no intercorrelation between A_4 and α_4 can be observed, which is a consequence of the parameters weak objective function sensitivity. To gain sufficient accuracy in the model calibration process, all the data in the experimental data sets (750/250), (1000/250) and (1500/250) were used. Three experimental data sets triple the function calls, when every individual needs to be evaluated for the respective initial values, which consequently multiply the computational time. The results from the calibration process are graphically presented in Figure 3, and the calibrated kinetic parameters are presented in Table 2. From Figure 3, it was concluded that the parameter estimation was successful, since the model predicted temporal average concentration and the observed measurements agree well. The calibration process was performed using 100 individuals and 30 iterations with the total computational time approaching six days. The results from the model calibration confirmed the validity of the inverse modeling methodology but, in principle, provided no information about the quality of the forward model itself. The forward model was validated against the experimental data set (2000/250), cf. Figure 3. The validations of the calibrated kinetic parameters show reasonable accordance. The explanation of the derivation of the model predicted and the experimental observed concentrations is out of scope of this paper.

5. Conclusions

In this paper, a methodology for catalytic converter parameter estimation has been presented. The PDE-based forward model was implemented in COMSOL Multiphysics, which provides a seamless interface into MATLAB. This functionality formed the basis of the inverse modeling framework.

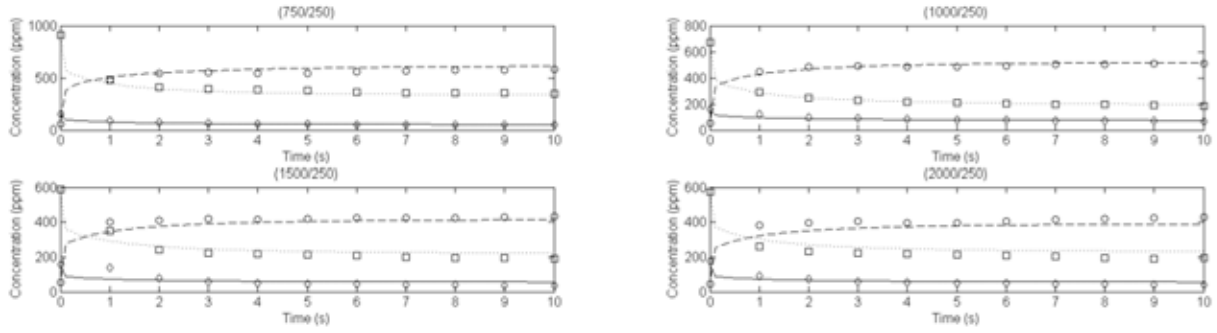

Figure 3. Comparison between the experimental observed and the model predicted outlet concentrations. Observed [NO_2] (○); [NO] (□); [C_3H_6] (◊). Predicted [NO_2] (---); [NO] (···); [C_3H_6] (—).

The ill-posed nature makes inverse problems challenging and special care must be taken in choice of optimization method to use. The applied evolutionary strategy was able to successfully solve the inverse problem associated with the mean field model. A possible drawback of ES methods, in spite of these good results, is computational effort required. However, it is well known that many stochastic methods, including ES, lend themselves to parallelization very easily, which means that this problem could be handled in reasonable time by suitable parallel versions.

A graphic method for confirming that the optimum has been reached was presented. From these scatter plots, the sensitivity of the calibration parameters could easily be studied as well as the parameter intercorrelation. Objective function sensitive calibration parameters showed trends in the scatter plot and they could be ranked according the size of the effect. This methodology has proven powerful when studying chemical pathways, but can easily be applied for solving a wide variety of PDE-based inverse problems.

6. References

1. C. Ericson, *Model Based Optimization of a Complete Diesel Engine/SCR System*, PhD thesis, Lund Faculty of Engineering, Department of Energy Science, Lund University (2009)
2. T.G. Chuah et al., Finite element study of three-way catalytic converter for NO_x abatement under transient isothermal condition, *International Journal of Engineering and Technology*, 1(2), 188 – 196 (2004)
3. B. Wickman et al., Modeling mass transport with microkinetics in monolithic NO_x storage and reduction catalyst, *Topics in Catalysis*, 42, 123-127 (2007)
4. R.E. Hayes et al., The effect of washcoat geometry on mass transfer in monolith reactors, *Chemical Engineering Science* 59, 3169 – 3181 (2004)
5. C. Brinkmeier, Automotive three-way exhaust aftertreatment under transient conditions – measurements, modeling and simulation, PhD thesis, Universität Stuttgart, (2006)
6. R. B. Bird, W. E. Stewart and E. N. Lightfoot, Transport Phenomena, John Wiley and Sons, New York (1960)
7. C. N. Satterfield, Mass Transfer in Heterogeneous Catalysis, MIT Press, Cambridge Mass. (1970)
8. R. J. Kee et al., Chemkin-III: A FORTRAN Chemical Kinetics Package for the Analysis of Gas-Phase Chemical and Plasma Kinetics, *Sandia National Laboratories Report SAND96-8216* (1996).
9. R. J. Kee et al., The Chemkin Thermodynamic Data Base, *Sandia National Laboratories Report SAND87-8215B* (1990).
10. M. Crocoll et al., Mean field modeling of NO oxidation over Pt/Al_2O_3 catalyst under oxygen-rich conditions, *Journal of Catalysis* 229, 480–489 (2005)
11. L. Olsson et al., Mean field modeling of NO_x storage on $Pt/BaO/Al_2O_3$, *Catalysis Today* 73, 263–270 (2002)
12. C. G. Moles et al Parameter Estimation in Biochemical Pathways: A Comparison of Global Optimization Methods, *Genome Research.*, 13, 2467-2474 (2003)
13. K. V. Price. An introduction to differential evolution. In D. Corne, M. Dorigo, and F. Glover, editors, New Ideas in Optimization, 79–108, McGraw-Hill, London, (1999)
14. R. Storn, System Design by Constraint Adaptation and Differential Evolution, *IEEE Transactions on Evolutionary Computation*, 3(1), 22–34 (1999)
15. K.V. Price et al., Differential Evolution – A Practical Approach to Global Optimization, Springer, Berlin (2005)
16. R. Storn et al., Differential Evolution - A Simple and Efficient Heuristic for Global Optimization over Continuous Spaces, Journal of Global Optimization, 11, 341–359 (1997)
17. F. Laurent et al., Modeling of NO_x adsorption over NO_x adsorbers, *Chemical Engineering Science,* 58, 1793 – 1803 (2003)
18. J.A. Dumesic et al., *The Micro kinetics of Heterogeneous Catalysis*, American Chemical Society, Washington (1993)
19. M. Cardiff et al., Efficient solution of nonlinear, underdetermined inverse problems with a generalized PDE model, *Computers & Geosciences*, 34, 1480– 1491 (2008)
20. T. R. Meisler, Methods to Solve Inverse Problems Using Comsol Multiphysics, *Excerpt from the Proceedings of the 2006 Nordic COMSOL Conference*, 1-6 (2006)
21. K. Papadakis, *Studies of heavy-duty diesel aftertreatment system based on the NO_x storage and reduction technology*, PhD thesis, Lund Faculty of Engineering, Department of Chemical Engineering, Lund University (2005)